Mirror Charge Radii and the Neutron Equation of State

B. Alex Brown

Mirror Charge Radii and the Neutron Equation of State

B. Alex Brown[1]

[1] Department of Physics and Astronomy and National Superconducting Cyclotron Laboratory,
Michigan State University, East Lansing, Michigan 48824-1321, USA

The differences in the charge radii of mirror nuclei are shown to be proportional to the derivative of the neutron equation of state and the symmetry energy at nuclear matter saturation density. This derivative is important for constraining the neutron equation of state for use in astrophysics. The charge radii of several neutron-rich nuclei are already measured to the accuracy of about 0.005 fm. Experiments at isotope-separator and radioactive-beam facilities are needed to measure the charge radii of the corresponding proton-rich mirror nuclei to a similar accuracy. It is also shown that neutron skins of nuclei with $N = Z$ depend upon the value of the symmetry energy at a density of 0.10 nucleons/fm^3.

The neutron skin is the difference in the root-mean-square (rms) radii of neutrons and protons in a nucleus. It was shown [1], [2] that the the neutron-skin of ^{208}Pb is proportional to the derivative of the neutron equation of state (EOS) $[E/N](\rho)$ near $\rho = 0.10$ nucleons/fm^3 in both non-relativistic and relativistic mean-field models. Further work, [3], [4], [5], [6], [7], showed that the neutron skins of ^{208}Pb and other neutron-rich nuclei such as ^{48}Ca are proportional to the derivative of the symmetry energy at nuclear matter saturation density ($\rho_0 = 0.16$ nucleons/fm^3):

$$L = 3\,\rho\,[\partial E_{\mathrm{sym}}(\rho)/\partial\rho]\,|_{\rho=\rho_0}, \qquad (1)$$

where $E_{\mathrm{sym}}(\rho) = [E/A](\rho) - [E/N](\rho)$ is the symmetry energy, and $[E/A](\rho)$ is the symmetric nuclear-matter EOS. L is important for the extrapolation of the EOS to the lower and higher densities needed for understanding neutron stars [8], [9], [10], [11].

If one has perfect charge symmetry, then the neutron rms radius in a given nucleus is equal to the proton charge radius in its mirror nucleus. This means that the neutron skin in a given nucleus can be obtained from the proton radii of mirror nuclei. In practice this can be done by measuring the charge rms radii and then making the relativistic and finite size corrections to deduce the point-proton rms radii. Charge symmetry is distorted by the Coulomb interaction in a way that can be calculated.

For example, with the Skx Skyrme energy-density functional (EDF) [12] without the Coulomb interaction, the results for ^{52}Cr for root-mean-square (rms) radius of neutrons, R_n, the rms radius of protons, R_p and the neutron skin, $\Delta R_{np} = R_n - R_p$ (in units of fm) are:

^{52}Cr : $R_n = 3.5844$, $R_p = 3.4961$ and $\Delta R_{np} = 0.0882$,

and the results for the mirror nucleus ^{52}Ni are:

^{52}Ni : $R'_n = 3.4956$, $R'_p = 3.5850$ and $\Delta R'_{np} = -0.0894$.

The proton radius difference of 0.0889 fm is essentially equal to the neutron skin in ^{52}Cr. (The small difference of about 0.0007 fm comes from the 0.13 percent difference of the proton and neutron mass in the kinetic energy operator. The uncertainty from this is an order of magniture smaller than the Coulomb effects discussed below.) The shell-model wavefunctions for the nuclei from ^{48}Ca to ^{56}Ni are dominated by the $0f_{7/2}$ orbital and I have assumed this configuration for the EDF calculations. (This is the configuration used for most EDF calculations of the ^{48}Ca neutron skin.) The EDF results presented here for charge radii and neutron skins should be extended beyond the $0f_{7/2}$ model, for example by including pairing in the EDF calculations. This may change the final numerical values a little, but not the trends and conclusions made here.

In this letter I show results from 48 Skyrme functionals. They start from the 12 functionals used in [13] that are among the "best" chosen in [14] out of several hundred from a variety of experimental criteria as well as some constraints from neutron-star properties. As shown in Table I, they cover a reasonable range of values for the symmetric nuclear-matter effective mass ($m^*/m = 0.70$-1.00) and incompressibility ($K_m = 212$-242 MeV) as compared to values extracted from the energy of the giant monopole resonances ($K_m = 217$-230 MeV) [15]. There are four versions of these 12 basic types. The first three versions are those from [13] where the isovector properties of the functionals were chosen to fit arbitrarily fixed values for the neutron skin of ^{208}Pb of 0.16, 0.20 and 0.24 fm. The result from this work was that the neutron EOS at a density of 0.10 neutrons/fm^3 was found to be $[E/N](0.10) = 11.4(1.0)$ MeV. The symmetry energy at this density is $E_{\mathrm{sym}}(0.10) = 25.5(1.0)$ MeV. In addition for this letter, I add a fourth version where the neutron skin of ^{208}Pb was constrained to be 0.12 fm. For all of these the neutron effective mass was fixed to be $m^*_n/m \approx 0.90$. In [16] it was found that a reasonable variation in the neutron effective mass had a small effect on the neutron skin.

The results for the neutron skins of ^{48}Ca and ^{208}Pb for these 48 functionals are plotted vs the slope of the
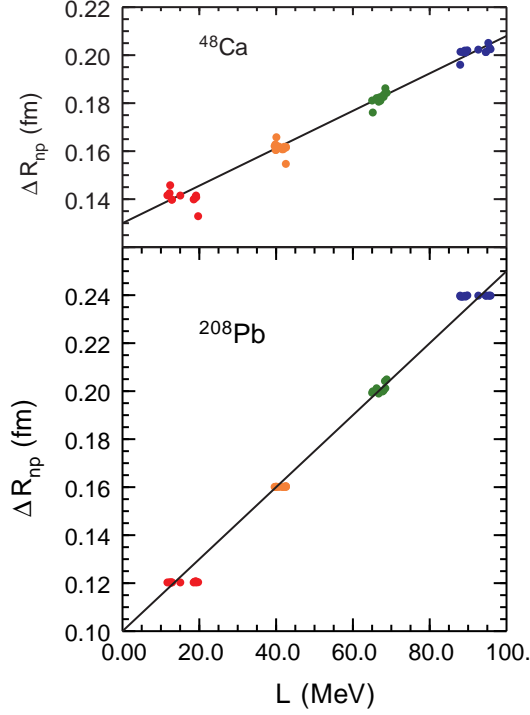
FIG. 1. Neutron skins for ^{48}Ca and ^{208}Pb for 48 Skyrme functionals plotted vs the slope of the symmetry energy, L The colors correspond to the constraints made for the neutron skin of ^{208}Pb: 0.12 fm (red), 0.16 fm (orange), 0.20 fm (green) and 0.24 fm (blue). The lines are to guide the eye.
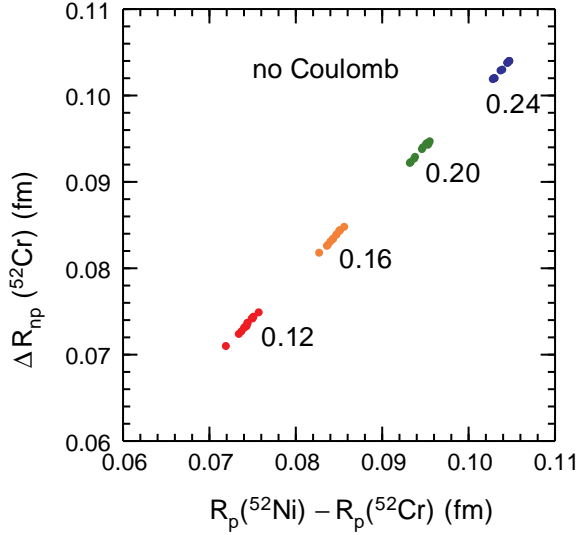

FIG. 2. Difference in the proton rms radii of the mirror nuclei ^{52}Ni and ^{52}Cr compared to the neutron skin of ^{52}Cr. Results are shown for the 48 Skyrme functionals discussed in the text but without the Coulomb interaction. The points are labeled according to their respective values for the neutron skin of ^{208}Pb ranging from 0.12 to 0.24 fm.
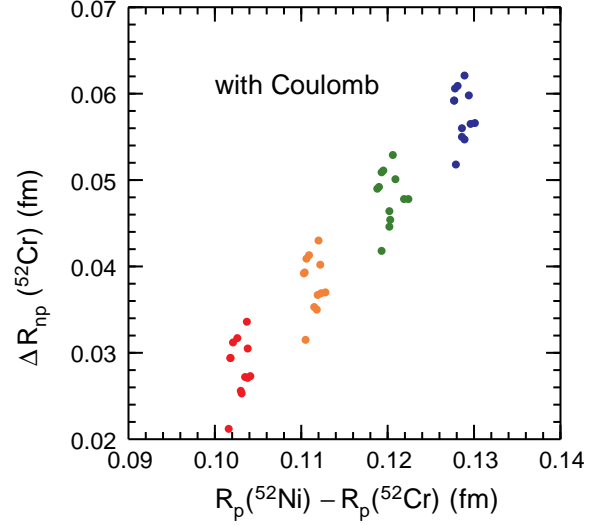

FIG. 3. Same as Fig. 2 but with the Coulomb interaction added.

TABLE I. Properties of the Skyrme functionals from [13]. The power of the density-dependent term in the Skyrme functional is $1+\sigma$. K_m is the symmetric nuclear-matter incompressibility and m^*/m is the effective mass.

name		σ	K_m MeV	$[m^*/m]$
KDE0v1	s3	1/6	216	0.79
NRAPR	s6	0.14	225	0.85
Ska25	s7	0.25	219	0.99
Ska35	s8	0.35	244	1.00
SKRA	s9	0.14	212	0.79
SkT1	s10	1/3	242	0.97
SkT2	s11	1/3	242	0.97
SkT3	s12	1/3	241	0.98
SQMC750	s15	1/6	228	0.71
SV-sym32	s16	0.30	237	0.91
SLy4	s17	1/6	224	0.70
SkM*	s18	1/6	218	0.78

symmetry energy in Fig. 1. As found previously the correlation between ΔR_{np} and L is high. There is a similar high correlation between ΔR_{np} and the slope of the symmetry energy at a lower density of 0.10 nucleons/fm^3 as found in [13].

The result for neutron skin of ^{52}Cr is plotted vs the mirror radius difference between the protons in ^{52}Ni and ^{52}Cr in Fig. 2. These were obtained with the 48 functionals, but with the Coulomb potential turned off. As expected, the points on this plot lie on a straight line. The values of the points are clustered according to the corresponding results for the neutron skin of ^{208}Pb as labeled in the figure.
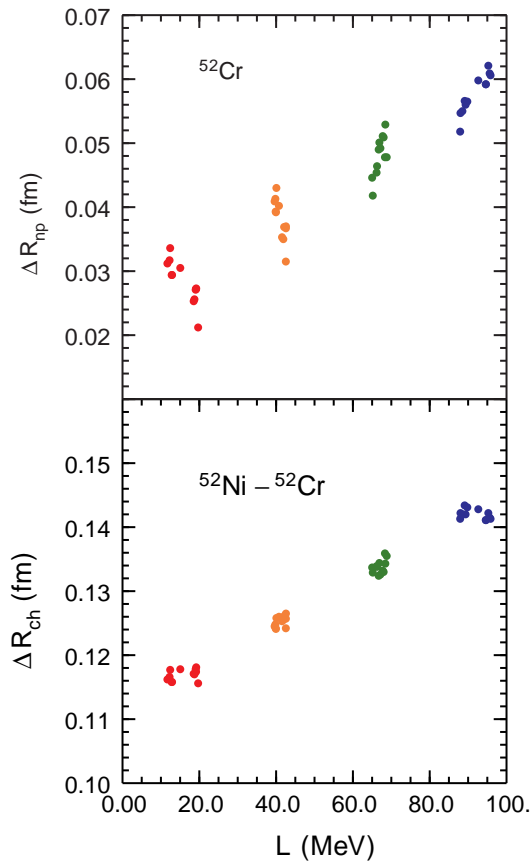
FIG. 4. The neutron skin of ^{52}Cr (top) and ΔR_{ch} for ^{52}Ni and ^{52}Cr (bottom) plotted vs the slope of the symmetry energy, L.

With the addition of the Coulomb interaction the Skx results are:

$$^{52}\text{Cr}: \quad R_n = 3.605, \ R_p = 3.562 \text{ and } \Delta R_{np} = 0.043,$$

and

$$^{52}\text{Ni}: \quad R'_n = 3.523, \ R'_p = 3.674 \text{ and } \Delta R'_{np} = -0.151,$$

with $R'_p - R_p = 0.112$ fm. There is an asymmetry in the neutron skin due to the fact that the Coulomb interaction pushes out the density of the protons relative to neutrons. The results for the 48 Skyrme functionals are shown in Fig. 3. The linear correlation becomes distorted. This is due to the self-consistent competition between the Coulomb interaction and the symmetry potential in the EDF calculations. The effective Coulomb interaction used in all of these EDF calculations reproduces the binding energy difference between ^{48}Ni and ^{48}Ca [17], and implicitly contains an approximation for the small charge asymmetry of the nuclear interaction [12], [18].

The effect of this distortion is mainly for the neutron skin. This is illustrated in Fig. 4 where the neutron skin
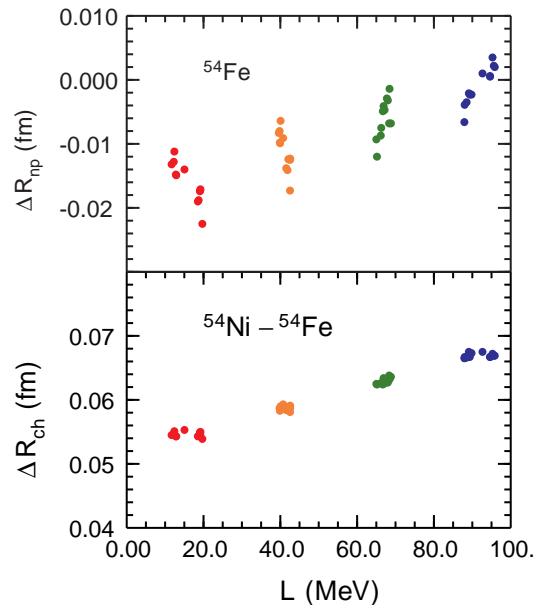

FIG. 5. The neutron skin of ^{54}Fe (top) and ΔR_{ch} for ^{54}Ni and ^{54}Fe (bottom) plotted vs the slope of the symmetry energy, L.
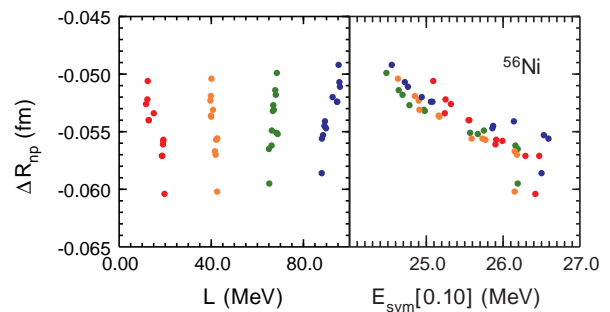

FIG. 6. The neutron skin of ^{56}Ni plotted vs the slope of the symmetry energy, L, (left), and vs the value of the symmetry energy at a density of 0.10 nucleons/fm^3 (right).

of ^{52}Cr and ΔR_{ch} for ^{52}Ni and ^{52}Cr are each plotted vs L. For this mass region, spread in the neutron skin due to the Coulomb distortion of about 0.010 fm is approximately independent of $\mid N - Z \mid$ (compare the scatter for ΔR_{np} in Fig. 6 with those of Figs. 4 and 5). For ^{56}Ni with $N = Z$ shown in Fig. 6, it is found that neutron skin is not determined L; rather the skin is correlated with value of the symmetry energy at a density of 0.10 nucleons/fm^3, $E_{\text{sym}}(0.10)$. Some of the scatter in the neutron skin of ^{48}Ca as a function of L shown in Fig. 1 comes from this dependence on $E_{\text{sym}}(0.10)$.

One concludes that ΔR_{ch} is correlated with $\mid N - Z \mid \times L$, whereas the neutron skin, ΔR_{np}, depends on both $\mid N - Z \mid \times L$ and $E_{\text{sym}}(0.10)$. When $N - Z$ becomes large the L dependence in ΔR_{np} dominates. Danielewicz has

studied this dependence in the framework of the nuclear mass formula with the addition of a surface symmetry energy term [19].

The charge radii are obtained from the proton radii by making corrections for the finite charge size of the proton and neutron and for the relativistic effects [20], [21]. Similar corrections must be considered for the neutron skin when the proton and neutron radii are deduced by electromagnetic probes of the charge (proton) and weak-charge (neutron) radii. The relativistic corrections are not negligible. From the measured charge radius of ^{48}Ca of 3.478(5) fm [22], the deduced proton radius is 3.417 (3.408) fm with (without) the relativistic corrections. The relativistic corrections were derived under the assumption of spin zero [20].

The extent to which mirror charge radii can be used to determine L depends on the accuracy to which they can be measured. The ideal case of ^{48}Ni vs ^{48}Ca ($| N - Z |=$ 8), but ^{48}Ni would be difficult to measure because it is hard to produce and decays by two-proton emission with a half life of $2.1^{+2.1}_{-0.7}$ ms [23]. Perhaps the next best case is that for ^{52}Ni vs ^{52}Cr with $| N - Z |= 4$ as discussed above and shown in Fig. 4. The measured charge radius of ^{52}Cr is 3.645(3) from [24] and 3.643(3) from [25]. Determination of the charge radius of ^{52}Ni to a similar degree of accuracy will require advanced rare-isotope beam (RIB) facilities such as FRIB. The results for ^{54}Ni and ^{54}Fe with $| N - Z |= 2$ are shown in Fig.5 . In this case the charge radius of ^{54}Fe is 3.694(5) [26]. The charge radius of ^{54}Ni may be obtainable in the near future at isotope separator or RIB facilities such as those presented in [27]. The obvious problem is that the dependence of ΔR_{ch} on L is linear in $| N - Z |$, and one would need higher precision experiments for smaller $| N - Z |$ in order to constrain the value of L to a similar level of accuracy.

We can consider existing data for lighter nuclei with the caveat that the EDF model approximation for these may become less reliable. The results for ^{34}Ar and ^{34}S with $| N - Z |= 2$ are shown in Fig. 7. For this case the orbital occupations for the EDF are taken from the sd wavefunctions obtained with the USDB Hamiltonian [28]. The experimental charge radius for ^{34}Ar is 3.3657(21)(92) fm where (21) is the statistical error and (92) is the systematic error [29] (the compiled value in [30] does not include the systematic error). The experimental charge radius for ^{34}S is 3.284(2) fm [31]. The radius difference of 0.082(9) fm is shown in Fig. 7. Compared to the EDF calculations it implies a value of $L < 60$ MeV. The error is dominated by the systematic error. One of the challenges of new experiments will be to reduce the systematic errors that depend upon calibrations and/or calculations of the mass- and field-shift coefficients that connect the atomic hyperfine structures to the change in charge radii [29], [27].

At present the electromagnetic determination of the neutron radius from parity-violating electron scattering
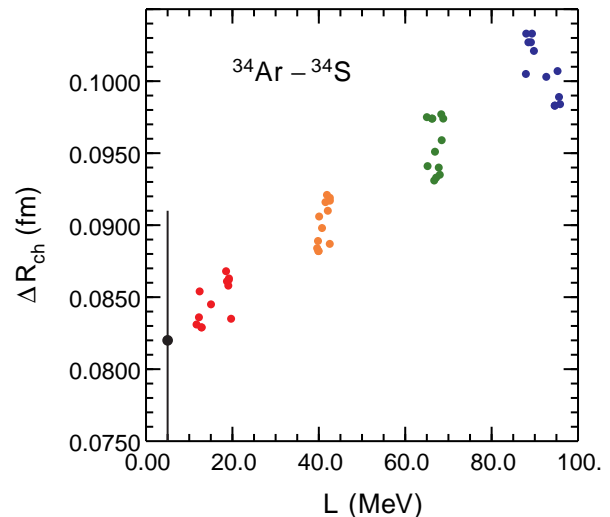

FIG. 7. ΔR_{ch} for ^{34}Ar and ^{34}S plotted vs the the slope of the symmetry energy, L. The experimental result (see text) for ΔR_{ch} is shown by the black point with an error bar near the y-axis.

has a large error. The ^{208}Pb neutron skin obtained from the PREX parity-violating electron-scattering experiment is $R_{np} = 0.302 \pm (0.175)_{exp} \pm (0.026)_{model} \pm (0.005)_{strange}$ fm [32], [33]. A PREX-II experiment has been approved that is expected to reduce the error bar to about 0.06 fm. Parity-violating experiments are planned for ^{48}Ca [34]. The precision that might be obtained from experiments on mirror charge radii is competitive with the planned JLAB experiment. The determination of the neutron density from strongly interacting probes depends upon one's confidence in understanding the strong interaction.

The correlations between the neutron-skins, the mirror charge radii, and the properties of the equations of state obtained with the Skyrme EDF should be compared to results obtained from ab-initio approaches based on chiral two- and three-body interactions [16], [35], [36] in order to constrain and extend the functional forms used for the EDF calculations.

In summary, I have shown that difference in charge radii, ΔR_{ch}, for mirror pairs is proportional to $| N - Z | \times L$ where L is the derivative of symmetry energy given in Eq. 1. In contrast, the neutron skin, ΔR_{np}, is proportional $| N - Z | \times L$ plus a term approximately independent of $| N - Z |$ that is proportional to $E_{sym}(0.10)$; the symmetry energy at a density of 0.10 nucleons/fm^3. When $| N - Z |$ is large (as in ^{48}Ca) the L term dominates. But as $| N - Z |$ goes to zero (as in ^{56}Ni) only the E_{sym} term remains. If the charge radii can be measured within an error of about 0.005 fm, the constraint on L from the mirror charge radii is better than that obtained from the planned parity-violating electron scattering ex-

periments. It will be important to have consistent results from several mirror pairs, and to take into account the systematic uncertainties, to be sure that there are no experimental or theoretical inconsistencies.

---

[1] B. A. Brown, Phys. Rev. Lett. **85**, 5296 (2000)
[2] S. Typel and B. A. Brown, Phys. Rev. C **64**, 027302 (2001).
[3] R. J. Furnstahl, Nucl. Phys. A **706**, 85 (2002).
[4] Lie-Wen Chen, Che Ming Ko, and Bao-An Li, Phys. Rev. C **72**, 064309 (2005).
[5] M. Centelles, X. Roca-Maza, X. Vinas, and M. Warda, Phys. Rev. Lett. **102**, 122502 (2009).
[6] M. Kortelainen, J. Erler, W. Nazarewicz, N. Birge, Y. Gao, and E. Olsen Phys. Rev. C **88**, 031305 (2013).
[7] P. G. Reinhard and W. Nazarewicz, Phys. Rev. C **93**, 051303 (2016).
[8] J. M. Lattimer and M. Prakash, Astrophys. J. **550**, 426 (2001).
[9] J. M. Lattimer and M. Prakash, Science **304**, 536 (2004).
[10] A. W. Steiner, J. M. Lattimer, and E. F. Brown, Astrophys. J. **765**, L5 (2013).
[11] K. Hebeler, J. M. Lattimer, C. J. Pethick, and A. Schwenk, Astrophys. J. **773**, 11 (2013).
[12] B. A. Brown, Phys. Rev. C **58**, 220 (1998).
[13] B. A. Brown, Phys. Rev. Lett. **111**, 232502 (2013).
[14] M. Dutra, O. Louenco, J. S. Sa Martins, A. Delfino, J. R. Stone, and P. D. Stevenson, Phys. Rev. C **85**, 035201 (2012).
[15] L. G. Cao, H. Sagawa and G. Colo, Phys. Rev. C **86**, 054313 (2012).
[16] B. A. Brown and A. Schwenk, Phys. Rev. C **89**, 011307(R) (2014); Rev. C **91**, 049902 (2015).
[17] B. A. Brown, Phys. Rev. C **43** 1513(R) (1991); Phys. Rev. C **44**, 924 (1991).
[18] B. A. Brown, W. A. Richter and R. Lindsay, Phys. Lett. **B483**, 49 (2000).
[19] P. Danielewicz, Nucl. Phys. A **727**, 233 (2003).
[20] W. Bertozzi, J. Friar, J. Heisenberg and J. Negele, Phys. Lett. B **41**, 408 (1972).
[21] B. A. Brown, S. E. Massen and P. E. Hodgson, J. Phys. G **5**, 1656 (1979)
[22] I. Angeli and K. P. Marinova, Atomic Data and Nucl. Data Tables **99**. 69 (2013).
[23] C. Dossat et al., Phys. Rev. C 72, 054315 (2005).
[24] H. D. Wohlfahrt, E. B. Shera, M. V. Hoehn, Y. Yamazaki, and R. M. Steffen, Phys. Rev. C **23**, 533 (1981).
[25] J. W. Lightbody et al., Phys. Rev. C **27**, 113 (1983).
[26] H. D. Wohlfahrt, O. Schwenker, G. Fricke, H. G. Andresen, and E. B. Shera, Phys. Rev. C **22**, 264 (1980).
[27] K. Minamisono et al., Phys. Rev. Lett. **117**, 252501 (2016).
[28] B. A. Brown and W. A. Richter, Phys. Rev. C **74**, 034315 (2006).
[29] A. Klein, B. A. Brown, U. Georg, M. Keim, P. Lievens, R. Neugart, M. Neuroth, R. E. Silverans and L. Vermeeren, Nucl. Phys. A **607**, 1 (1996).
[30] Nuclear Data and Nuclear Data Tables **99**, 69 (2013).
[31] L. A. Schaller et al., Phys. Rev. C **31**, 1007 (1985).
[32] S. Abrahamyan, Z. Ahmed, H. Albataineh, K. Aniol, D. S. Armstrong, W. Armstrong, T. Averett, B. Babineau, A. Barbieri, V. Bellini, *et al.* Phys. Rev. Lett. **108**, 112502 (2012).
[33] C. J. Horowitz, Z. Ahmed, C.-M. Jen, A. Rakhman, P. A. Souder, M. M. Dalton, N. Liyanage, K. D. Paschke, K. Saenboonruang, R. Silwal, *et al.*, Phys. Rev. C **85**, 032501 (2012).
[34] C. J. Horowitz, K. S. Kumar, and R. Michaels, Eur. Phys. J. A **50**, 48 (2014).
[35] G. Hagen et al., Nature Phys. **12**, 186 (2015).
[36] J. W. Holt and N. Kaiser, Phys. Rev. C **95**, 034326 (2017).